Sindh Univ. Res. Jour. (Sci. Ser.) Vol.46 (4):423-428 (2014)

SINDH UNIVERSITY RESEARCH JOURNAL (SCIENCE SERIES)

Computation of blood flow separation and reattachment length on Stenosed artery using Finite Element Method

A. A. SHAIKH*, M. S. CHANDIO++

Institute of Mathematics and Computer Science, University of Sindh, Jamshoro

Received 8th June 2014 and Revised 15th November 2014

Abstract: In this article, attention is focused on laminar blood flow simulation in large stenosed arteries. Here, blood flow separation and reattachment points are computed at a range of *Reynolds* numbers with various percentage of occlusion in the artery. The simulation is carried out under axisymmetric steady laminar flow on a segment of diseased artery with obstruction ratios ranging from 20% to 80% at selected *Reynolds* numbers from 10 to 1000. The Finite Element Method is employed for the computation of reattachment length finite element meshes are generated using commercial software I-DEAS. We found that the predicted reattachment length increases with grid refinement and is in good agreement with experimental results. It is also observed that increasing *Reynolds* number has also affected the reattachment length, which shows increasing trend. The numerical calculations are performed up to *Re* = 1000 in order to maintain stability of the algorithm and to avoid divergence of the solution. SitPak Finite Element Method (FEM) is employed to solve the System of governing equations.

Keywords: Blood flow Simulation, re-attachment length, stenosis, finite element method

1. INTRODUCTION

Deposition of cholesterol and other fatty tissues along human arterial walls can form a constriction and therefore restrict the blood flow. The deposition of plaques causes the walls of the artery thicker. Due to this the openings of the artery become narrows that subsequently reduce blood flow. This build-up can lead to stroke or heart attack or the dysfunction of other organs. Experimental and numerical techniques have been used by many scholars to investigate the formation of plaque and its size. These scholars in their research work have also computed shear stress at various Reynolds numbers with different obstruction ratios in the diseased carotid arteries.

Clinical and postmortem studies have shown that the Atherosclerotic lesions on human blood vessel walls do not develop randomly and do not occur throughout the circulation but rather local at certain selected location in the arterial tree, such as the branching sites and curved segments of large arteries (Shunsuke *et al.,* 1996).

Baghdadi (2002 and Salzar *et al*. 1995) have reported that millions of people worldwide are affected by the atherosclerosis that leads to diseases as heart failure, brain stroke and long-term disability.

According to WHO reports (2006,2008), if this this trend continues, the number of deaths due to heart failures and strokes, may rise to 20 million by 2015.

Boyd *et al.*, (2006) used a 2D carotid artery model to investigate the validity of Newtonian viscosity near wall shear stress in a two-dimensional carotid artery model.

Golpayeghani *et al*. (2008) in their numerical work have used incompressible Navier-Stokes equations. They studied the effects of local stenosis in carotid artery. The parameters of interest they focused upon were the time-dependent velocity profile in various regions and flow separation and reattachment points on the wall. They also investigated wall shear stress variation in whole artery and compared the results with non-Newtonian fluid.

In a study by Rockman *et al*. (2013) reported that about various races around the world who are at high risk for stroke. They further investigated that the occurrence of Carotid artery stenosis (CAS) also differs by race.

They studied and analyzed the prevalence of CAS in people of various races by vascular screening examinations. The people they chosen were Cau-casian (90%), African American(3.1%), Hispanic (2.4%), Asian (1.9%), and Native American (2.8%) individuals. They found that occurrence of CAS in males (4.2%) was larger in comparison to female (3.4%). Rockman *et al.* (2013) further reported in their paper that Native Americans were the highest who suffered from CAS in

++Corresponding Author M. Saleem chandio email: mschandio@hotmail.com

*Department of Basic Sciences and related studies, MUET, Jamshoro, asifali_1968@hotmail.com

both male and female irrespective of age. Caucasian people were second highest who suffered CAS for all ages and in both sexes. In contrast to Native American, African American males had the lowest occurrence of CAS in almost all age groups. Their study also found that Asian females are less affected by CAS in comparison to females of other people discussed above in all age groups.

Numerical simulation of blood flow explores various characteristics of cardiovascular diseases and subsequently, contributes to devise potential diagnostic procedures. It offers a non-invasive means of obtaining detailed flow patterns associated with disease by supplying information beyond that which is available in an experimental study. The particular role of wall geometry together with the type and character of the flow can be defined widely in a numerical study.

Large numbers of theoretical and experimental studies are carried out based on blood flow simulations on a stenosed artery for the understanding of blood flow disorder in the presence stenosis.

Ellahi *et al.,* (2014) studied Blood flow of micro polar fluid through composite stenosis in an artery with permeable wall. They, further, investigated that flow impedance increases by increasing stenosis height, while decrease in impedance has been observed by increasing slip parameter and tube length.

Pankaj and Surekha (2013) developed a mathematical model to compute the effects of stenosis in an artery using power-law model. They used analytical approach and found that the pressure drop and shear stress increases as the size of the stenosis increases for a given non-Newtonian model of the blood.

Sapna (2011) considering non-Newtonian blood flow, investigated that the size of constriction largely effects the blood flow and shear stresses. She found that the flow resistance increases with increasing size of the stenosis. Similar observations were found for wall shear stresses.

Sankar (2011) has analyzed blood flow simulation in narrow arteries. In his work, he considered pulsatile flow of two phase model for asymmetric model. He found increase in wall shear stress is directly proportional to the height of the stenosis. Similar trend was observed in pressure drop. They also found the wall shear stress increases non-linearly with the increase of the axial distance.

Misra and Shit (2006) investigated non-Newtonian bahaviour of blood through and Analytical solutions and found that the flow resistance was large at the throat of the stenosis and smaller at the ends of stenosis.

The partial occlusion of arteries due to atherosclerosis is one of the most frequently occurring abnormalities in humans (Young and Frank, 1973). This local obstruction is called a stenosis. The stenosis definition is the ratio of the minimum cross-sectional area, A_1, to the unobstructed lumen area A_0. The commonly used term “percent stenosis” is defined as:

$$\%\ \text{Stenosis} = \left(1 - \frac{A_1}{A_0}\right) \times 100$$

A one to 39 percent stenosis is considered mild, 40 to 59 percent is considered moderate, 60 to 79 percent severe, and 80 to 99 percent critical. A stenosis may be caused by the impingement of extravascular masses, but is more frequently the result of intravascular atherosclerotic plaques which develop at the wall of the artery or an arterial prosthesis and go forward in to the lumen. The development of a localized arterial stenosis may lead to disordered blood flow within the downstream area of the constricted regions (Rabby *et. al.,* 2014). The degree of perturbation is strongly influenced by the severity of the stenosis, and for moderate to severe stenoses, highly disturbed regions of flow distal to the stenosis commonly occur under physiological flow conditions (Yongchareon and Young 1979).

In addition to other parameters, reattachment length, and turbulence are the specific fluid mechanics parameters that are affected by the presence of a stenosis.

This article elucidates that our investigation is first motivated by an interest in detailed fluid dynamics associated with a stenosis at various stages of disease development in an artery.

The flow simulation results from this segment of the study are applied to theoretically discuss the prediction on the hemodynamic performance of polyester protein-impregnated arterial prostheses after implantation at different stages of capsule development. Finally, the computational flow simulation was made with a severer, 86% stenosis for selected R*e* numbers ranging from 5 to 633.

Comparing the result obtained in this study with experimental result (Ainser et al, 2000) clearly showed that the initializing of instability and transition from laminar to turbulent flow developed at relatively small R*e* numbers (compared to its traditional value of 2300 for pipe flow) called critical Reynolds number, indicating that the laminar flow simulation failed in the case of the severe stenosis and high Reynolds number. From a clinical viewpoint, several important problems such as post-stenotic dilatation are consideration of the disordered flow downstream of the stenosis.

GEOMETRY AND BOUNDARY CONDITIONS

The geometry and boundary conditions for various degrees of axisymmetric stenosis are show in Figure 1. The form of stenosis was chosen as an abrupt expansion. The axial velocity boundary conditions were specified by UZC. In this model, including the symmetry line in the flow region, the symmetry boundary condition was set on this line. The radial velocity component URC was constrained to zero and the axial velocity component was left free. The diameter ratios are 0.9, 0.7 and 0.5 corresponding to the 20%, 50% and 75% stenosis, respectively. These values are in non-dimensional form relative to the main artery diameter. A parabolic velocity profile with a non-dimensional maximum velocity equal to two was imposed at the inflow which was located 10D (*i.e*., unobstructed diameter, D) upstream of the stenosis. The assumption of a parabolic profile was that fully developed flow was attained before the flow reached the stenosis. At the outflow boundary, radial velocity (URC) was explicitly imposed at zero, resulting in zero normal and tangential stresses at the outflow boundary. The outflow boundary was located 15D downstream. Therefore, the total length in the horizontal direction was 30D from inlet boundary.

The no-slip boundary conditions were imposed on the wall. For the purpose of computation the six node triangular elements are used with fine meshes near the walls along the stenosed region.

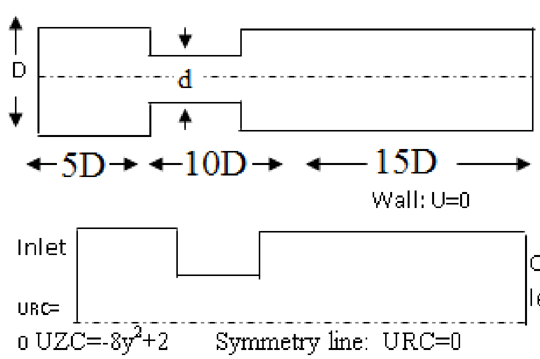

Fig. 1: Geometry of an arterial segment with a d% local stenosis and boundary conditions.

GOVERNING EQUATIONS

Equation of momentum and the equation of continuity may be represented as governing equations for an incompressible, isothermal, steady, and laminar flow.

$$\rho \frac{\partial u}{\partial t} = \nabla . \mathrm{T} - \rho u . \nabla u - \nabla p \qquad (1)$$

$$\nabla . u = 0 \qquad (2)$$

where ‘t’ is time, **u**(x, t) fluid velocity, ‘p’ is pressure and ‘ρ’ is the fluid density. For Newtonian Flow

$T = 2\mu_0 D$,

$$\text{where } D = \frac{1}{2}\left(\frac{\partial u_i}{\partial u_j} + \frac{\partial u_j}{\partial u_i}\right)$$

Equation (1) can be written as (3)

$$\rho \frac{\partial u}{\partial t} = \mu_0 \nabla^2 u - \rho u . \nabla u - \nabla p$$

For steady state, we get

$$\mu_0 \nabla^2 u - \rho u . \nabla u - \nabla p = 0 \qquad (4)$$

The density ρ and the dynamic viscosity μ_0 of the blood are taken as 1.05 g/cm^3 and 0.035 g/cm sec, respectively.

NUMERICAL METHOD AND FINITE ELEMENT ANALYSIS

Finite element method discretized the domain into elements. Taylor-Galerkin procedures are used for time/space discretization. Instead of Crouzeix-Raviart element, the Taylor-Hood triangular element is used as shown in figure 2:

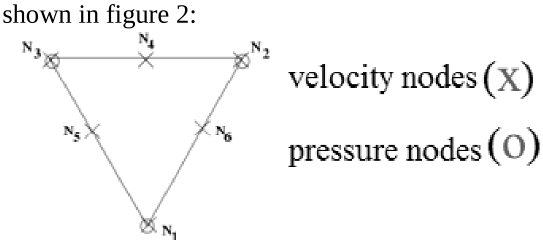

Fig. 2: the Taylor-Hood triangular element, six velocity nodes and three pressure nodes.

Applying finite element Taylor-Galerkin procedures for time/space discretization The fully-discrete semi-implicit Taylor-Galarkin/Pressure-Correction system of equations may be expressed in matrix form as (Chandio and Webster 2002):

$$\left(\frac{2\,\mathrm{Re}}{\Delta t} + \frac{1}{2}S\right)\left(U^{n+\frac{1}{2}} + U^n\right) = \left\{-\left[S + \mathrm{Re}\,N(U)\right]U + L^T P\right\}^n$$

$$\left(\frac{\mathrm{Re}}{\Delta t} + \frac{1}{2}S\right)\left(U^* - U^n\right) = -\left[S\,U + L^T P\right]^n + \left[\mathrm{Re}\,N(U)U\right]^{n+\frac{1}{2}}$$

$$K\left(P^{n+1} - P^n\right) = -\frac{2}{\Delta t} L U^*$$

$$\frac{1}{\Delta t} M\left(U^{n+1} - U^*\right) = \frac{1}{2} L^t \left(P^{n+1} - P^n\right)$$

Here M is mass-matrix, S diffusive matrix, $N(U)$ convection matrix, L is pressure-gradient matrix and K is pressure-stiffness matrix. In Matrix form these can be expressed as follow:

$$M_{ij} = \int_{\Omega} \phi_i \, \phi_j \, d\Omega$$

$$N(U)_{ij} = \int_{\Omega} \phi_i \, \phi_1 U_1 \nabla \phi_j d\Omega$$

$$((L_k)_{ij}) = \int_{\Omega} \psi_i \frac{\partial \phi_j}{\partial \phi_k} d\Omega$$

$$K_{ij} = \int_{\Omega} \nabla \psi_i \, \nabla \psi_j \, d\Omega$$

$$S_{ij} = \int_{\Omega} \nabla \phi_i \, \nabla \phi_j \, d\Omega$$

An iterative method is used to solve the resulting mass matrix equation.

3, RESULTS AND DISCUSSION

Grid dependence tests are performed on 80% stenosis with five grids downstream of the stenosis height, consisting of coarse mesh1, coarse mesh1, dense mesh1 and dense mesh2 having 1×8×16, 1×16×16, 2×8×16 and 2×16×16, elements respectively, (see figure 3). The test focused primarily on the reattachment length. The numerical computed reattachment length compared with experimental value (see Figure 6) is presented in Table 1. The predicted reattachment lengths increased with grid refinement approaching the experimental length.

Table 1 Comparison of non-dimensional numerical reattachment lengths with different grid sizes.

Meshes/Experiment	Reattachment L_a/D
Experiment	8.7
Present, Coarse Mesh 1	7.7
Present, Coarse Mesh 2	8.1
Present, Fine Mesh 1	8.4
Present, Fine Mesh 2	8.45

The reattachment lengths did not show a significant variation between two finest grids, therefore, further mesh refinement was not performed because of prohibitive computing time. Hence, all subsequent computations are done with a 2×16×16 elements on the stenosis height corresponding to 18800 elements for the entire geometry. *Reynolds* numbers are selected in the range of 10 to 1000 where R*e* number was based on the bulk velocity at the inlet boundary and the unobstructed artery diameter. The Newton-Raphson numerical method was used to solve the nonlinear equation solution. The convergence criteria used was the reduction of filed residuals to 1000000th of their original value.

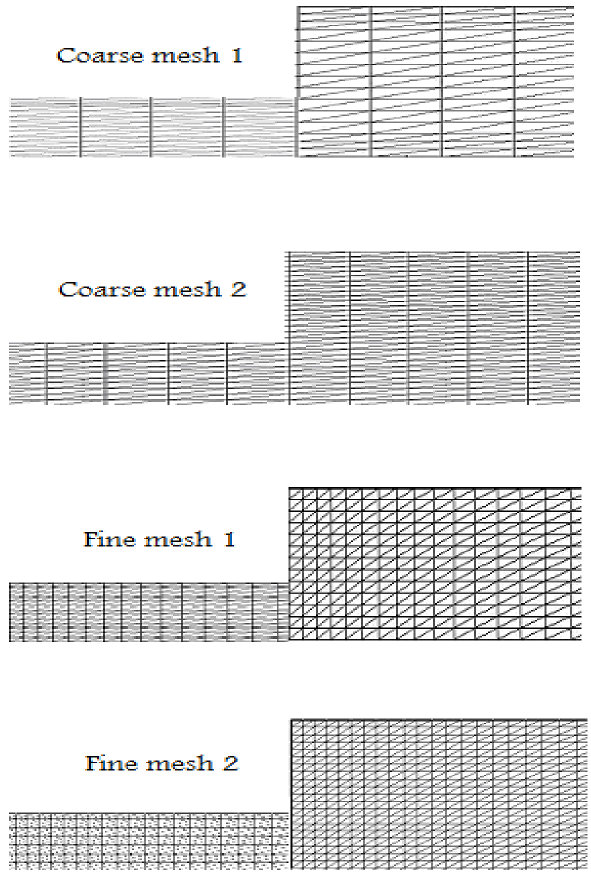

Figure 3: The finite element meshes around 80% stenosis. Top to bottom are shown coarse mesh1, coarse mesh2, Fine mesh1 and Fine mesh2.

SEPARATION AND RE-ATTACHMENT POINT

Theoretical analyses and experimental observations have indicated that a region of separated flow will commonly downstream from a stenosis at low R*e* numbers (Chahed et. al. 1991, Tobin and Chang,1976). The zone of separation is region of relatively low shear stress therefore, the fluid inside the vortex region may act differently than the fluid outside.

Of particular interest here was the R*e* number at which separation was initiated and the location of the separation and reattachment points. At low Reynolds numbers, the separation occurred close to the end of the occlusion in the flow direction, and gradually the separation point shifted upstream. In contrast, the point of reattachment moved far away downstream with increasing R*e* number. The length of the laminar vortex elongated with increasing R*e* number. Figure 4.a and 4.b illustrate the calculated streamlines for different Reynolds number. The vortex length was determined by the axial distance of the reattachment point from the stenosis end. The letter *R* indicates the location for the reattachment point.

The variation in reattachment length *(L_a/D)* was plotted as a function of upstream Reynolds number and is shown in Figure 5. The length of the vortex distal to the stenosis *(d/D)* had a highly significant effect on vortex length. For instance, at a R*e* of 1000, the relative vortex length distal to the stenosis with a constriction *(d/D)* of 0.9 (20% stenosis) was only approximately 0.48D, yet for the stenosis with a constriction of 0.5, the relative vortex length increased to 43.86D at the same Reynolds number. Interestingly, however, the computation shows that the stenosis length *L/D* had very little effect on the size of the vortex. The hypothetical results were all confined to laminar flow. Young and Frank (1973) have reported that separated flow is very unstable; it was therefore not surprising to find that perturbations develop in a constricted artery at low R*e* number. The computational results presented here do not provide the flow instabilities that occur at a "critical" Reynolds number. The critical R*e* number is the value at which flow instability is first observed.

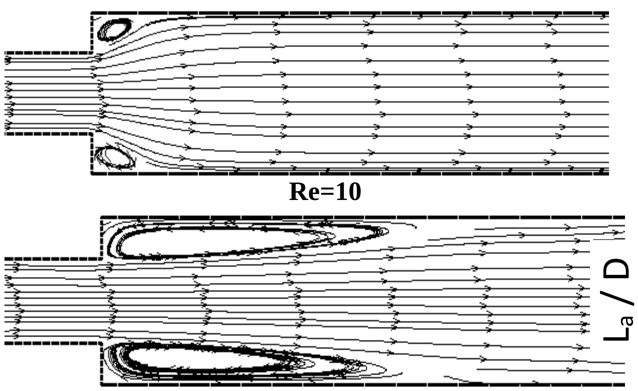

Fig. 4.a: Laminar flow recirculation region downstream of the 50% stenosis: Re=10 and Re=100.

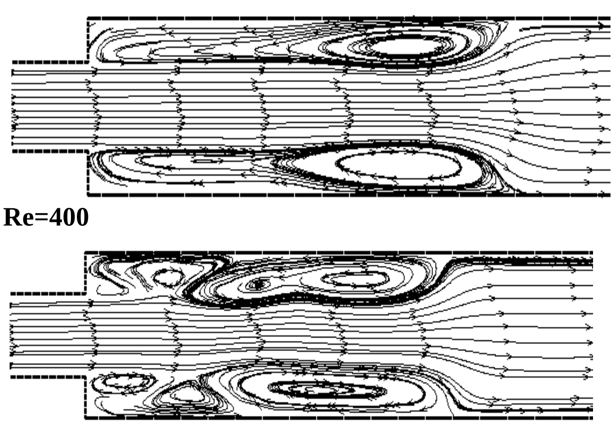

Fig. 4.b: Laminar flow recirculation region downstream of the 50% stenosis: *Re*=400 and *Re*=1000

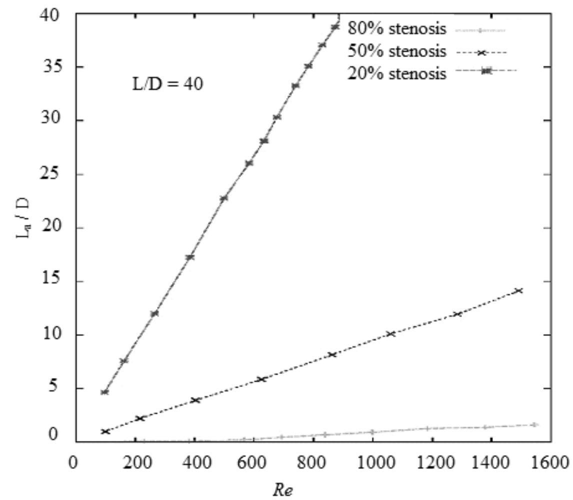

Fig. 5: The variation in reattachment length L/D as a function of the upstream Reynolds number

The variation of reattachment length as a function of upstream Reynolds number obtained by (Back and Roschke,1990) is shown in Figure 6.

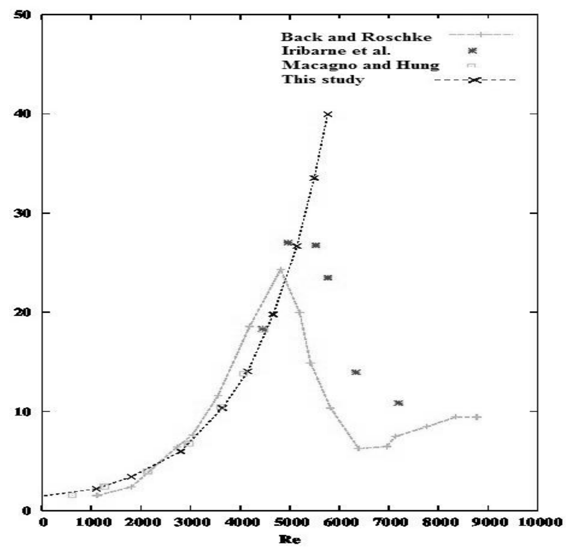

Fig. 6: The variation of reattachment length as a function of upstream Reynolds number. The numerical results of this study (80% stenosis and L/D = 20) are compared with the experimental data.

The numerical flow simulation under laminar flow for the same degree of stenosis (80%) and Reynolds number ranging from 5 to 633 was performed and compared with the experimental results. The comparative results on the variation s in reattachment length as a function of the upstream Reynolds number are also given in Figure 5. it was observed that the critical Reynolds number, the reattachment length continued to increase, in contrast to the experimental results which showed a decreasing reattachment length with increasing Reynolds number.

4. CONCLUSION

The results of this simulation are presented at various streamline functions and reattachment length downstream from the stenosis. A useful parameter to find the reattachment point was the length of the recirculation region that was characterized by its length L_a, the distance between the outlet of the stenosis and the reattachment point where the derivation of spatial velocity reduced to zero at the wall. As a result of this recirculation zone, there were negative velocities and therefore an inversion of the direction of the streamlines. *The Reynolds number* is an important factor in the flow as it depended above all on the value of the flow rate. We have emphasized here its impact on the length of the recirculating zone. It is also observed that length of laminar vortex elongated with increasing Reynolds numbers.

In the present study, it is observed that for mild stenosis, for small *Re* number no separation is evident and for large Re flow separation occurred. However, flow behaves as laminar. Further separation point becomes unstable where transition towards turbulence occurs and persists well beyond reattachment point.

REFERENCES:

Ainser, A., C. Carrot, J. Guillet, I. Sirakov (2000), Transient viscoelastic analysis of falling weight experiment, XIIIth Int. Cong. Rheol., Vol.2, 259-261, Cambridge, UK, 2000

Back L. H. and E. J. Roschke (1972), Shear layer flow regimes and wave instabilities and reattachment lengths downstream of an abrupt circular channel expansion, ASME J. Appl. Mech. Vol. 39: 677-681.

Baghdad L. (2002) Template-Based Finite Element Mesh Generation From Medical Images, Department of Medical Biophysics, M.Sc. Thesis, The University of Western Ontario London, Ontario, Canada

Boyd J., J.M. Buick and S. Green (2006) Application of the Lattice Boltzmann Method to non-Newtonian flow in a carotid artery model, Australian Institute of Physics 17th National Congress 2006–Brisbane.

Chahed N., Péronneau P, Delouche A, Diebold B (1991), Velocity profiles and streamlines of a revolution post-stenotic flow, Biorheology, Vol. 28(5):383-400.

Chandio M. S. and M. F. Webster (2002), Numerical simulation for viscousfree surface flows for reverse roller- coating, International Journal of Numerical Methods for Heat & Fluid Flow, Vol.12(4): 434-457.

Ellahi R, S. U. Rahman, M. Mudassar Gulzar, S. Nadeem and K. Vafai (2014), Mathematical study of non-Newtonian Micropolar fluid in Arterial Blood flow through composite Stenosis, Applied Mathematics and Information Science, Vol. 8 (4),1567-1573.

Global status report on non communicable diseases, (2006), World Health Organization, Geneva.

Global atlas on cardiovascular disease prevention and control, (2008) World Health Organization, Geneva.

Golpayeghani A. T., S. Najarian, M. M Movahedi (2008), Numerical Simulation of Pulsatile flow with Newtonian and non-Newtonian behavior in arterial stenosis, Iranian Cardiovascular Research Journal; 1:167-174.

Mathur P. and S. Jain, (2013), Mathematical Modelling of non-Newtonian Blood flow though Artery in stenosis, Advances in Applied Mathematical Biosciences, Vol. 4(1),1-12.

Misra J. C. and G. C. Shit (2006), Blood flow through arteries in pathological state: A theory study, International Journal of Engineering Science, Vol. 44, 662-671

Rabby M. G., Shupti S. P, and Mola M. (2014) Pulsatile Non-Newtonian Laminar Blood Flows through Arterial Double Stenoses, Journal of Fluids, Vol.2014:1-13

Rockman C.B., H. Hoang, Y. Guo, T. S. Maldonado, G. R. Jacobowitz, T. Talishinskiy, T. S. Riles, and J. S. Berger, (2013), The prevalence of carotid artery stenosis varies significantly by race, J/ Vas. Surg, Vol.57(2):327-337.

Sankar D. S. (2011), Two Phase non-linear model for blood flow in asymmetric and axisymmetric stenossed arteries, International Journal of Non-Linear Mechanics, vol. 46, 296-305.

Shah S. R. (2011), Mathematical Analysis of Blood flow though atherosclerotic arterial segment having non-symmetric mild stenosis, International Journal of Research in Pure and Applied Physics, Vol. 1(1),pp: 1-5

Shunsuke E., S. Yasunori , K. Takeshi (1996), Flow patterns in dog aortic arch under a steady flow condition simulating mid-systole, Heart and Vessels, Vol.11(4):180-191.

Tobin R. J. and I. D. Chang (1976), Wall pressure spectra scaling downstream of stenosis in steady tube flow, J. Biomechanics., Vol.9(10):630-640.

Yongchareon W, and Young D. F. (1979), Initiation of turbulence in models of arterial stenosis, J. of Biomechanics, Vol.12(3):185-196.

Young D. F. and Frank Y. T. (1973), Flow characteristics in models of arterial stenoses I. Steady flow, J. BioMechanics, Journal of Biomechanics Vol. 6(4): 395–402.